Soft-x-ray fluorescence spectra of III-V phosphides BP, GaP, and InP

L. Lin, G. T. Woods, and T. A. Callcott
Department of Physics and Astronomy, The University of Tennessee, Knoxville, Tennessee 37996-1200
(Received 27 September 2000; published 14 May 2001)

The valence band electronic structures of the III-V phosphides BP, GaP, and InP were investigated using soft x-ray fluorescence spectroscopy and compared with band structure calculations using full-potential linearized augmented plane wave method based on density functional theory. The P $L_{2,3}$ spectra of these phosphorus compounds are reported and compared with the calculated $(s+d)$-local partial densities of states (LPDOS's). For BP, the B K spectrum is also reported. Generally good agreement is obtained between the spectra and calculated LPDOS's. Two other interesting results were found. The normally suppressed P L_1 spectrum was observed in resonance with the B K spectrum of BP. Also, strong resonant inelastic x-ray scattering was observed at the Ga $M_{2,3}$ edge associated with energy loss to local electronic excitations from the Ga d states, permitting the Ga d states to be accurately located with respect to other band features.

DOI: 10.1103/PhysRevB.63.235107 PACS number(s): 78.70.En, 71.20.Mq

I. INTRODUCTION

The semiconducting III-V phosphides have attracted considerable interest in solid state physics because of their useful electronic properties. These materials are significant for the production of electronic devices, e.g., GaP has been used as a material for light emitting diodes (LED's), and InP is especially important for the design of transferred-electron devices. Because of their extensive applications, a great deal of experimental and theoretical[1–16] effort has been devoted to the study of the energy band structures and related properties of these materials. However, most of the soft x-ray emission[17–19] studies were carried out in the 1970's and 1980's using electron excitation. Recently, the P K emission spectra of III-V phosphides and a few transition-metal phosphides have been measured.[20]

In the present work, we used soft x-ray fluorescence (SXF) spectroscopy to study the element- and angular momentum-selected densities of states in the valence bands of the III-V phosphides BP, GaP, and InP. The P $L_{2,3}$ spectra of these phosphorus compounds were measured, and their band structure calculations were carried out within the density functional theory.[21,22] The comparison between the P $L_{2,3}$ spectra and the corresponding $s+d$ local partial densities of states (LPDOS's) of these phosphorus compounds is reported. A generally good agreement between calculation and experiment is obtained. Besides this, two other interesting results are found. A surprising result is that the normally suppressed P L_1 spectrum was observed in resonance with the B K spectrum. Also, resonance inelastic x-ray scattering (RIXS) was observed at the Ga $M_{2,3}$ edge associated with energy loss to local electronic excitation from the Ga $3d$ levels. This measurement permits the d states to be located accurately with respect to the valence bands of the system.

II. EXPERIMENTAL PROCEDURES

The experiments described here were performed at the soft x-ray fluorescence end-station of beamline 8.0 of the Advanced Light Source (ALS) at Lawrence Berkeley National Laboratory (LBNL). This beam line consists of a 5-cm-period undulator and a spherical grating monochromator, which delivers x rays in the energy range between 100 and 1000 eV with high resolution and intensity. The light from the undulator is passed through a high-resolution spherical grating monochromator and then directed to the sample chamber. The photon flux from the monochromator is estimated to be 10^{13} photons per second into a focused line of 200 μm$\times$2 mm with a maximum resolving power of 10 000. For the more modest resolving powers of $\leqslant$1000 used for soft x-ray fluorescnece studies, the monochromator delivers fluxes of approximately 10^{14} photons/sec into a focused line of 200 μm$\times$2 mm aligned with the entrance slit of the emission spectrometer.

The soft x-ray fluorescence end-station consists of a Rowland circle grating spectrometer with a photon-counting area detector and an ultrahigh vacuum sample chamber. The sample chamber has an XYZ-θ sample manipulator and a sample load lock for quick sample exchange. The grating chamber utilizes four interchangeable gratings to permit coverage of the energy range from 40 eV to 1000 eV with excellent resolution. The grazing incidence spectrometer has a fixed entrance slit rigidly mounted on a flange in the sample chamber. The photon-counting area detector is mounted tangent to the Rowland circle. It is scanned on the Rowland circle by a precision XYZ-θ table that permits different Rowland circles (5 m and 10 m) to be utilized for low- and high-energy spectra. The detector consists of a stack of microchannel plate output to a shaped resistive sheet, which provides true photon-counting detection with a measured resolution of less than 50 μm. The pixels of the 25-mm-diameter detector are binned electronically to provide a resolution of approximately 100 μm in the dispersion direction and 1.5 mm in the transverse direction. The 1.5-mm strips are shifted by software to remove curvature in the spectra. The detector is limited to a total count rate of about 10^5 counts/sec, so that it is not suitable for use with intense spectra. For the phosphorus spectra at about 135 eV, the spectrometer (with a 100-μm entrance slit, a 600-line/mm, 10-m

TABLE I. Parameters used in the LPDOS calculations for BP, GaP and InP.

	BP	GaP	InP
Lattice type	fcc	fcc	fcc
Lattice constants	a_0=4.538 Å (=8.58 a.u.)	a_0=5.4505 Å (=10.30 a.u.)	a_0=5.8687 Å (=11.09 a.u.)
Muffin-tin radius R_{MT} (a.u.)	B: 1.85	Ga: 2.0	In: 2.0
	P: 1.85	P: 2.0	P: 2.0
No. *k* points/BZ	3000	3000	3000
No. plane waves	170	278	336
No. Kohn-Sham eqs.	8	18	24
Total charge/unit cell	20	36	64
Cutoff parameter (a.u. Ry)	8.0	8.0	8.0
Core/valence cutoff energy (Ry)	-6.0	-6.0	-6.06
Core electrons	B: [He]	Ga: [Ar]	In: [Ar]$3d^{10}4s^2$
	P: [Ne]	P: [Ne]	P: [Ne]
Valence electrons	B: $2s^2 2p$	Ga: $3d^{10}4s^2 4p$	In: $4p^6 4d^{10}5s^2 5p$
	P: $3s^2 3p^3$	P: $3s^2 3p^3$	P: $3s^2 3p^3$

Rowland circle) has an energy resolution of about 0.4 eV. The optical plane of the emission spectrometer is in the horizontal plane and the sample rotation axis is vertical, so that spectra are excited with *p*- rather than *s*-polarized light. Further details of the properties of the SXF spectrometer are described elsewhere.[23]

If the spectrum covers a wider energy range than can be acquired in a single scan, then the detector is moved along the Rowland circle and several overlapping scans are acquired. These overlapping spectral segments are then joined smoothly. Calibration of the spectrometer in the energy range of present experiments are based on known x-ray edge features. The exciton peak of hexagonal BN at 188 eV was used as a calibration for the P $L_{2,3}$ and B *K* spectra reported here.

The materials studied in this paper were purchased from the Alfa/Aesar Research Chemicals. Because many of these materials are sensitive to moisture, samples were prepared in nitrogen bags with extra care to reduce the chance of oxidation before measurements could take place. Powder samples were first poured into a pellet die and then pressed by a hydraulic pump at pressures about 8000 psi to form small pellets to improve the emission intensity. The exposure time was shortened by keeping the freshly made samples in the nitrogen bag until they were ready to be moved to the sample transfer arm and then transferred to the sample chamber when pressure in the sample chamber is pumped down to workable pressure. The working pressure is 1×10^{-8} torr or better. Unwanted oxygen contamination of the samples was readily detected from the presence of sharp emission lines associated with the phosphate complex.

III. CALCULATIONS

III-V phosphides crystalize in the cubic zinc-blende structure, and each atom is tetrahedrally coordinated by atoms of the opposite kind. The atom positions of these phosphorus compounds are listed in Table I. In the past, various calculational methods have been applied by different investigators to study the electronic structures of a number of important semiconductors including III-V phosphides. Among them, Cohen and Bergstresser[7] used the empirical pseudopotential method and calculated the band structures and pseudopotential form factors for a number of semiconductors of the diamond and zinc-blende structures; speculating that a purely local pseudopotential technique could not yield satisfactory results, Chelikowsky and co-workers[9,10] employed an empirical nonlocal pseudopotential method and recalculated the band structures and density of states of several diamond and zinc-blende semiconductors. But these methods used only sp^3 basis and did not include the contribution of *d* state in the calculations.

To take into account the *d* state contribution in the calculations, we used an all-electron full-potential approach with a linearized augmented plane wave (LAPW) basis, the full-potential (FLAPW) method, as implemented in the WIEN97 code.[24] The exchange and correlation were treated with the generalized gradient approximation (GGA) using the parametrization of Perdew *et al.*[25] Core electrons were treated relativistically, and all the valence electrons were treated self-consistently. For the purpose of reducing the computational load, all of the band structure calculations presented here were carried out by first converging the total energy to within 10^{-4} Ry with 1000 *k* points in the Brillouin zone (BZ). Using this new starting potential, they were then reconverged again to within 10^{-4} Ry with 3000 *k* points in the BZ. In addition, in all of the calculations, data were normalized to set the energy at the top of the valence band equals to 0 eV. Local partial densities of states were determined by means of the modified tetrahedron method of Blöchl *et al.*[26] It is called LPDOS because it is selective to elements (local)

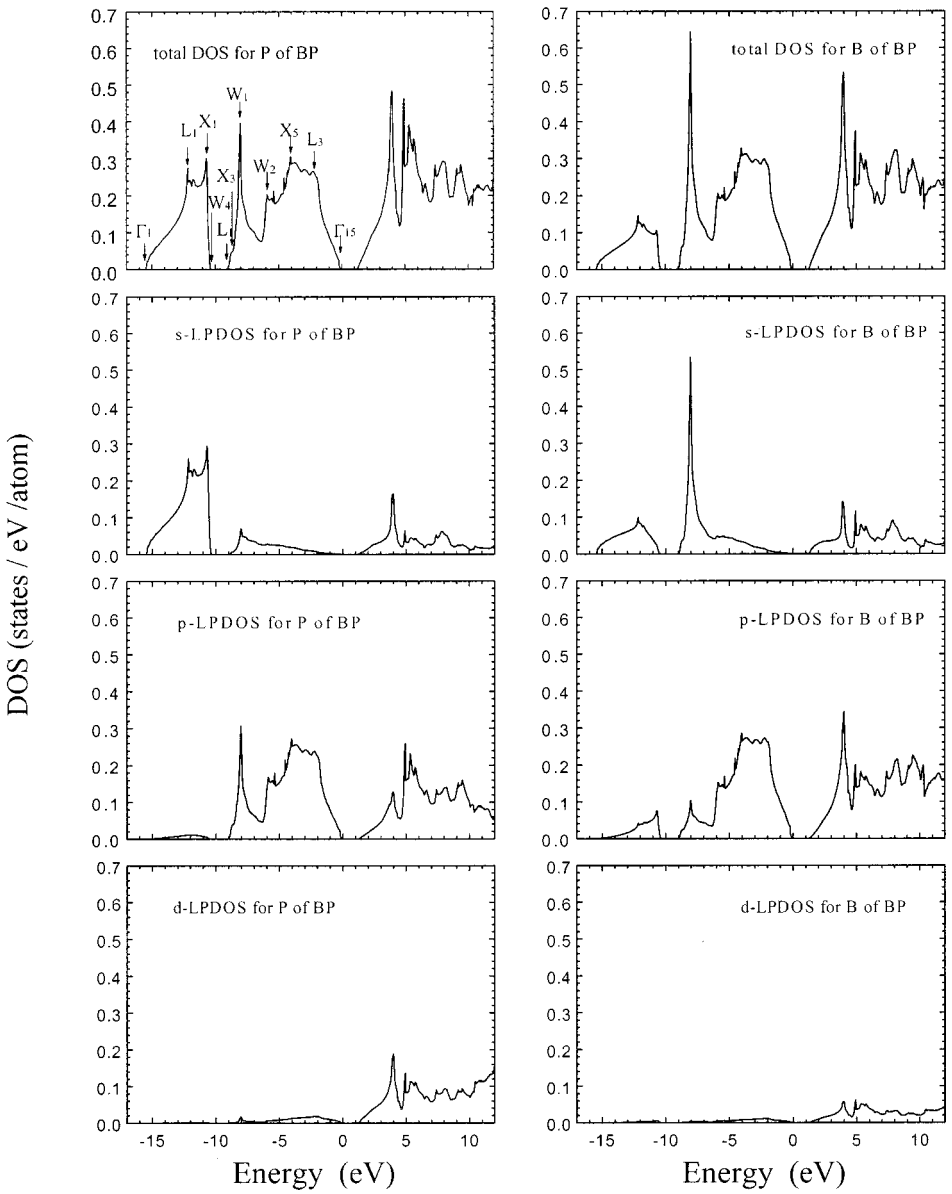

FIG. 1. Calculated local partial densities of states for BP.

and selective to angular momentum (partial). The element- and angular-momentum-selected LPDOS's are shown for BP, GaP, and InP in Figs. 1–3. The location of critical points in the calculated valence band are shown for the total DOS for P in BP in Fig. 1.[9,27]

IV. RESULTS AND DISCUSSION

A. Phosphorus $L_{2,3}$ spectra of BP, GaP, and InP

In Figs. 4 and 5, the P $L_{2,3}$ soft x-ray fluorescence spectra are compared with the corresponding $s+d$ local partial density of states of BP, GaP, and InP. These experimental spectra are excited well above the threshold so that they are normal fluorescence spectra that can be appropriately compared to the calculated LPDOS's. These spectra are similar to one another with minor differences. The peak in the lower valence band (LVB) of the normal fluorescence spectra is derived from the phosphorus 3*s* states, and the peaks in the upper valence band (UVB) are derived primarily from states of *s*-like symmetry associated with the covalent bonding between phosphorus *p* and cation *s* states in these compounds. These spectral features change little with increasing excitation energies, and there is no threshold effect observed in these phosphorus $L_{2,3}$ spectra.

In Fig. 4, two well-resolved peaks in the lower valence band are observed in the phosphorus $L_{2,3}$ spectrum of BP. These two peaks in the LVB are separated by about 1.2 eV. This splitting in the low-energy peak is also shown in the density of states calculation of BP. The splitting in this low-energy peak is not clearly resolved in P $L_{2,3}$ spectra of GaP or InP, reported in Fig. 5. From the LPDOS calculations of BP, GaP, and InP, we can see that the splitting in low-energy

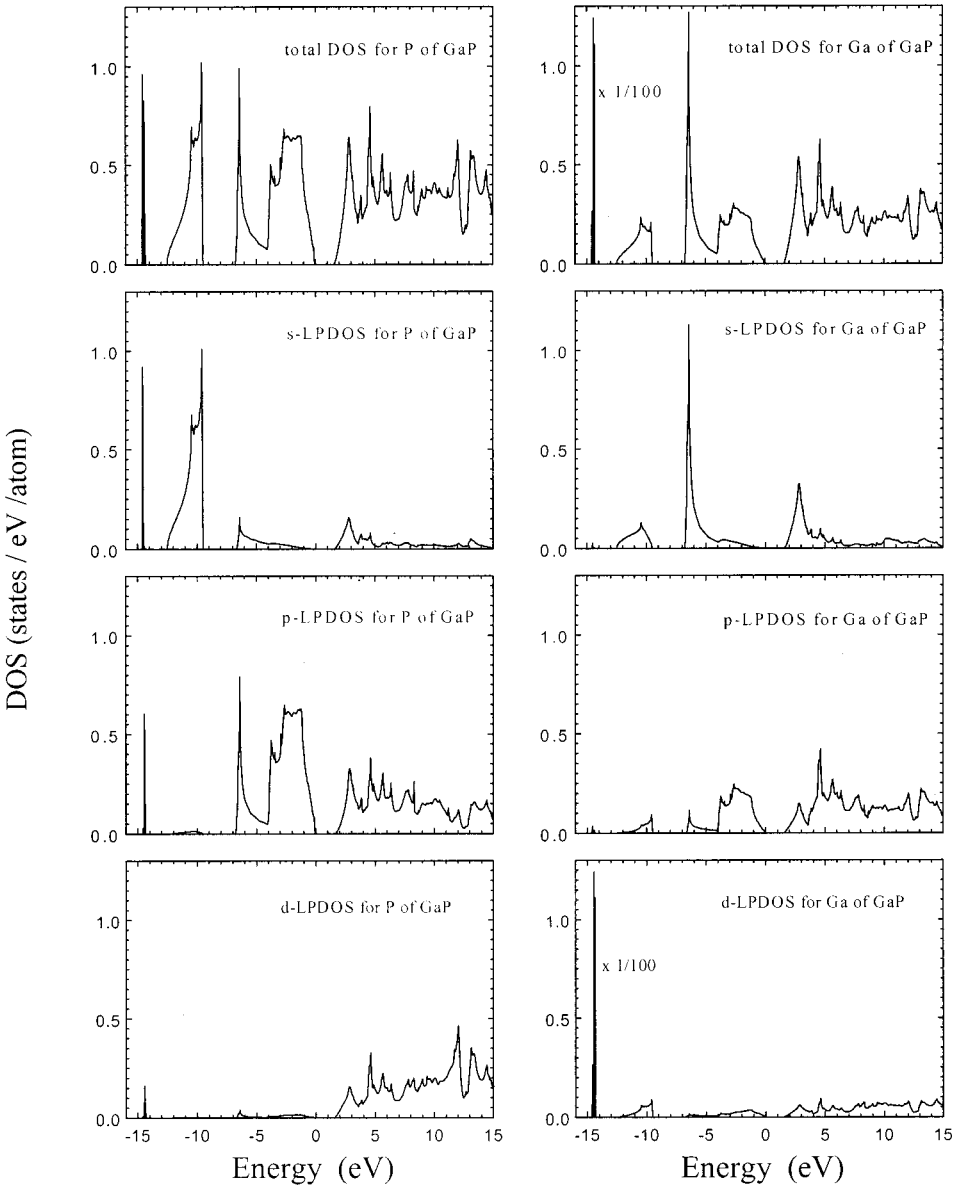

FIG. 2. Calculated local partial densities of states for GaP.

peak in BP is greater than that in GaP or InP. Therefore, it is reasonable not to resolve the splitting in P $L_{2,3}$ spectra of GaP and InP.

The P $L_{2,3}$ SXF spectra of both GaP and InP show a high-energy shoulder on the lower valence band. The shoulder is not well resolved in BP but broadens the upper edge of the spectra spaced about 1 eV above the peak value. This shoulder results from the 1-eV spin-orbit splitting of phosphorus $2p_{1/2}$ and $2p_{3/2}$ core levels. More specifically, the main peak in LVB results from phosphorus $3s$ electrons filling the $2p_{3/2}$ states, and the high-energy shoulder results from $3s$ electrons filling the $2p_{1/2}$ states.

Both gallium and indium have filled d shells, and their d bands are located several electron volts below the lower valence band. The valence band gap of several electron volts between the lower and upper valence bands is related to the lack of an inversion center in the zinc-blende lattice and the electronegativity difference between the cations (Ga, In) and phosphorus.[16] Since the d electrons in phosphides of gallium and indium lie at deeper positions below the valence band, they do not participate directly in the bonding. However, because of the repulsive effect of the d bands of Ga and In, which lies near the bottom of the valence band, the main peaks in the $L_{2,3}$ spectra of phosphides of these metals have a smaller binding energy than those of the other III-V phosphides.

The P $L_{2,3}$ spectra for the three compounds are compared in Fig. 6. We observe that the peaks at the LVB shift toward the high energy from BP to GaP to InP with increasing ionicity of compounds. In general, two interesting trends can be established from an overview of the SXF spectra of these III-V phosphides. First, when the lattice constant increases

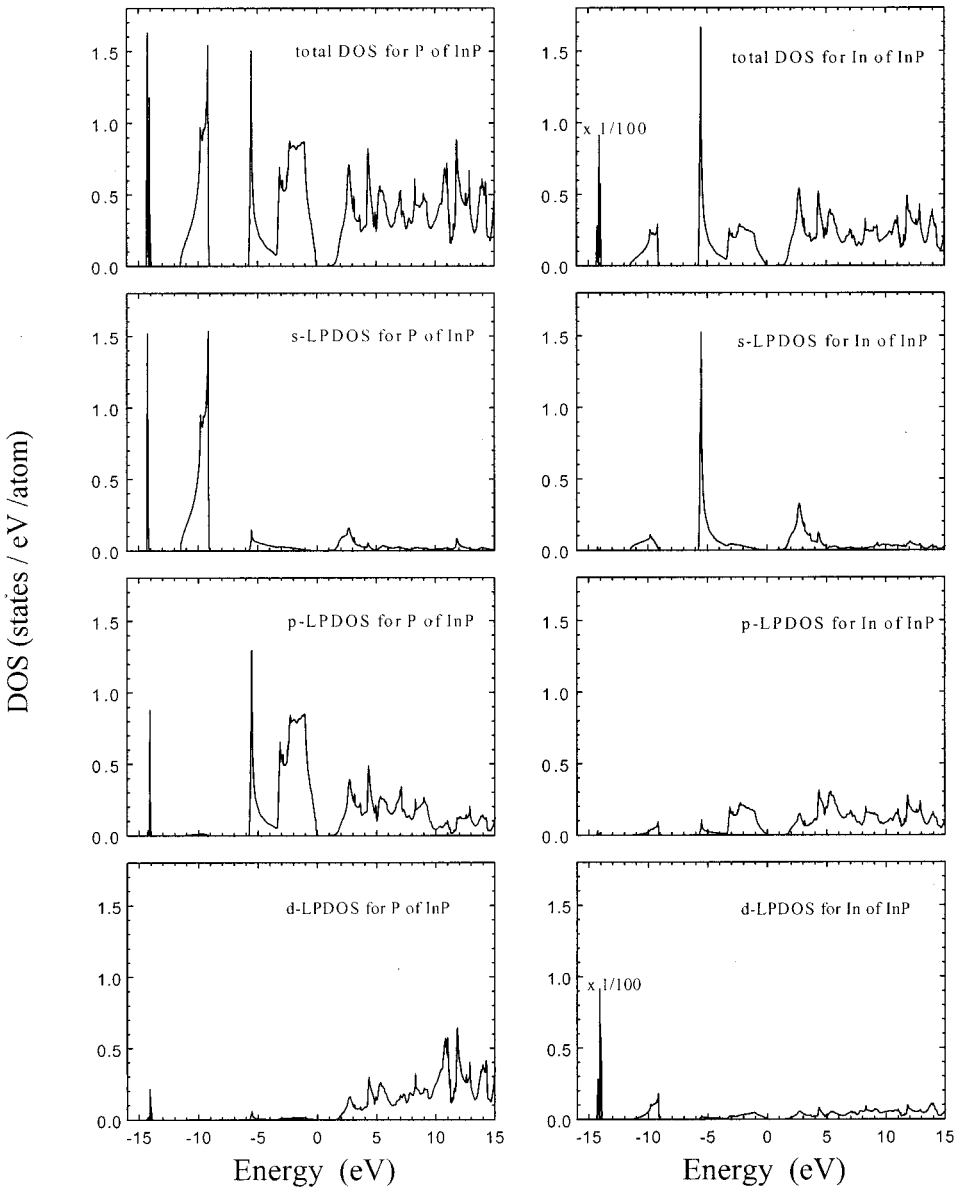

FIG. 3. Calculated local partial densities of states for InP.

the valence bandwidth decreases. Second, when the compound becomes more ionic, the gap occurring in the valence band increases. In the calculations by Chelikowsky and Cohen,[10] these trends were indicated for the III-V gallium and indium compounds as well, and the second trend was attributed to the changes in the antisymmetric part of the pseudopotential and ionicity.[28]

Peak positions in the spectra are compared with equivalent features of the LPDOS calculation in Table II. Tabulated energies are binding energies measured from the top of the upper valence band of the L_3 spectrum. This energy is taken to be 1.0 eV below the extrapolated position of the $L_{2,3}$ spectrum in order to account for the contributions of the L_2 spectrum. These positions are indicated in the table for E_a. From Table II, we can see that a good measure of the bandwidth of the UVB is given by E_{e-a}. The location of the LVB is given by E_{f-a}. The calculated heteropolar gap E_{f-e} is smaller than the experimental value.

B. Boron *K* spectra of BP

BP shows especially interesting structure changes in soft x-ray fluorescence spectra at the boron *K* edge as shown in Fig. 7. The structural features are those labeled as *a* through *f* in Fig. 4, which can be directly associated with density of states features seen in the band structure calculations. We observe that the spectral features change dramatically within 6 eV of the threshold. At excitation energy $h\nu_{in}=188.3$ eV, the fluorescent peak starts to show. As the excitation energy increases from 189.3 eV to 191.2 eV, the peak indicated in the figure by a dashed line tracks the elastic peak and shifts toward higher energy; the energy separation between this

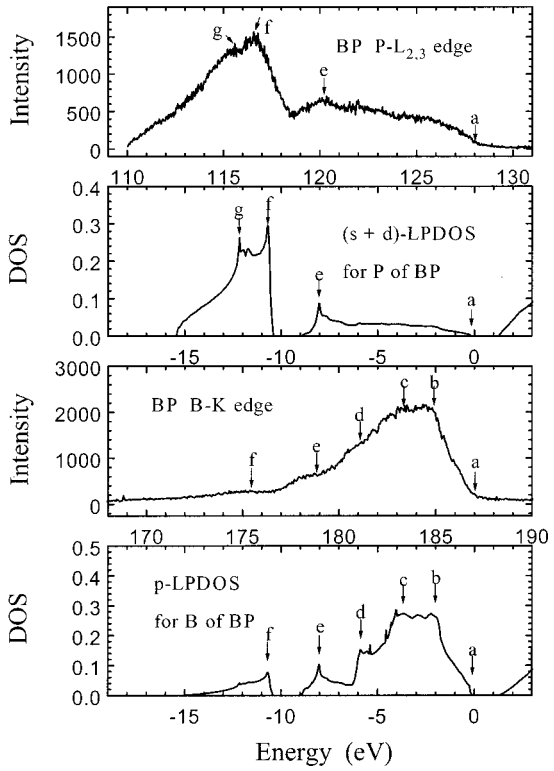

FIG. 4. Comparison of P $L_{2,3}$ and B K spectra of BP with calculated LPDOS's.

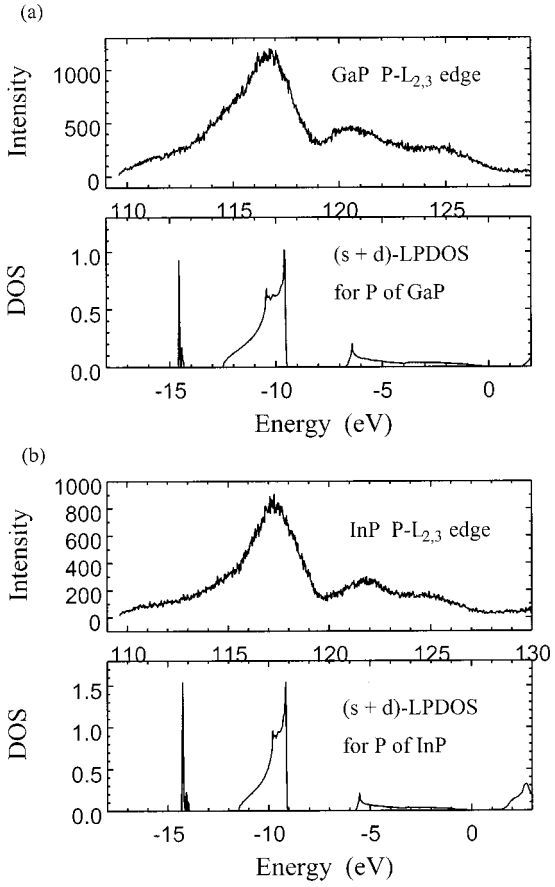

FIG. 5. Comparison of P $L_{2,3}$ spectra of (a) GaP and (b) InP with calculated LPDOS's.

peak and the elastic peak is about 6.8 eV. This tracking of elastic and inelastic features is the signature of the RIXS process, which is discussed further in the following section of this paper. We also notice that at $h\nu_{in}=191.2$ eV, the elastic peak resonates strongly, the intensity of the peak located at 186.1 eV (arrow) is enhanced. Then, at $h\nu_{in}=193.0$ eV, a second resonance is observed in the elastic peak and another intensity enhancement of peak (*e*) located at 178.6 eV (arrow) is observed.

The first resonance in the elastic peak at $h\nu_{in}=191.2$ eV is associated with excitation to a core-exciton state near the bottom of the conduction band minimum. We believe that the second resonance in the elastic peak and the accompanying enhancement of the emission peak (*e*) is associated with the presence of the L_1 threshold for phosphorus, which lies 1 eV above the B K edge. Two features identify the spectrum excited at 193 eV as being associated in part with a P L_1 spectrum. First, a second resonance appears in the elastic peak 1 eV above the B K resonance, and second, the strongly enhanced peak (*e*) is also strongly intensified in the p LPDOS of P shown in Fig. 1. Normally an L_1 emission spectrum is not observed for phosphorus and other light elements, but is suppressed by nonradiative deexcitation processes. In this case, however, since the phosphorus L_1 edge is only 1 eV higher than boron K edge, we believe that resonance coupling between the B K and P L_1 excitations greatly enhances radiative decay to the P L_1 level in this material. It may be significant that this peak in the P p states is strongly hybridized with B s states as may be seen in the LPDOS's of Fig. 1.

C. Gallium $M_{2,3}$ spectra of GaP

Although no significant changes are observed at the P $L_{2,3}$ edge, the situation is very different near the Ga $M_{2,3}$ edge where inelastic scattering dominates the observed spectra. In the resonant inelastic x-ray scattering process, the incident

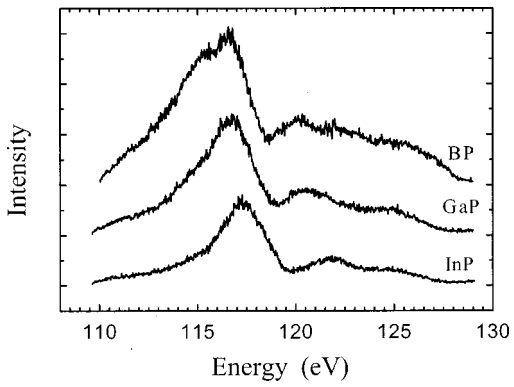

FIG. 6. Comparison of P $L_{2,3}$ spectra among BP, GaP, and InP.

TABLE II. The energy separations between peak positions in P $L_{2,3}$ spectra of III-V phosphides in experiments and calculations.

	BP (B *K* edge)	BP (P *L* edge)	GaP (P *L* edge)	InP (P *L* edge)
E_{b-a} expt. (theory)	2.2 (1.8)			
E_{c-a} expt. (theory)	3.9 (3.6)			
E_{d-a} expt. (theory)	6.0 (5.8)			
E_{e-a} expt. (theory)	8.4 (7.9)	7.8 (7.8)	6.1 (6.1)	4.8 (5.2)
E_{f-a} expt. (theory)	11.8 (10.6)	11.4 (10.5)	9.9 (9.3)	9.5 (8.9)
E_{g-a} expt. (theory)		12.4 (11.9)	NA[a] (10.1)	NA[a] (9.5)
E_{f-e} expt. (theory)	3.4 (2.7)	3.6 (2.7)	3.8 (3.2)	4.7 (3.7)

[a]Not available.

photon loses energy to an electronic excitation, and is detected at a lower energy, coincident in energy with the normal x-ray emission process. An example of this scattering process was reported by Zhou *et al.*[29] at the Zn $M_{2,3}$ edge in ZnS and Zn_2SSe. This scattering is described as a second-order perturbation effect.[30–32] One of the important features of the RIXS process is that the energy losses are determined only by the energy difference between initial and final states,

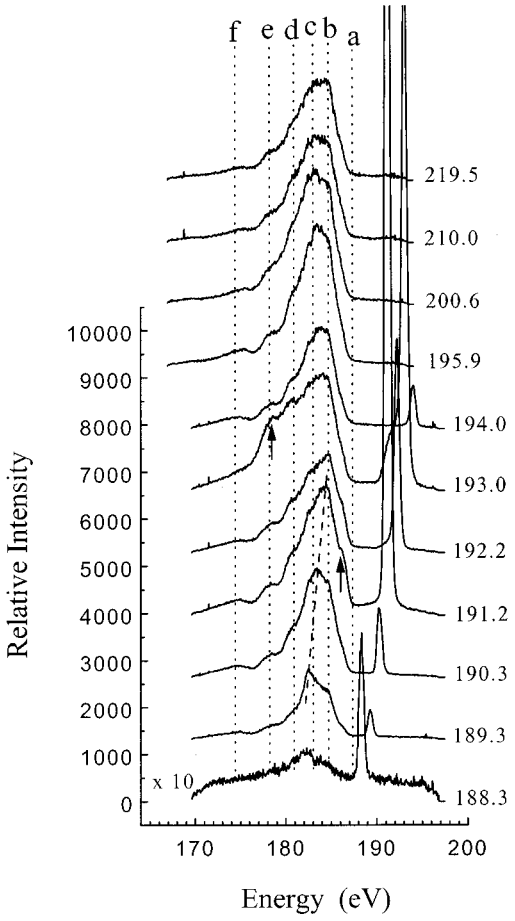

FIG. 7. B *K* spectra of BP excited near threshold. The excitation energy is indicated on the right.

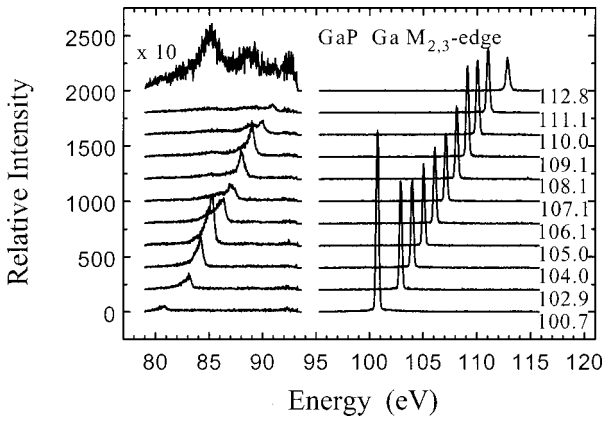

FIG. 8. Resonant inelastic x-ray scattering at the Ga $M_{2,3}$ edge in GaP. The excitation energy is indicated on the right-hand side of the elastic (right) peaks.

independent of the intermediate states. Also the spectral widths are affected only by the lifetime broadening in the final state of the system and are not limited by the lifetime of the core hole that exists in the intermediate state, whereas the spectral intensity is determined by matrix elements for the intermediate states.

Spectra described from the inlastic scattering process are observed at the Ga $M_{2,3}$ edge in GaP and are presented in Fig. 8. In this figure, the elastic peaks are plotted on the right-hand-side of the figure and the inelastic peaks on the left. All spectra shown are normalized to the incident photon flux with the excitation energies labeled next to the elastic peaks. For display purposes, the normal fluorescence spectrum is multiplied as indicated. The energy separation between the measured elastic and inelastic peaks is 19.8 eV. This energy loss is associated with an electronic excitation process produced by an excitation from Ga 3*d* states to a relatively narrow final state. The 1 eV width of this inelastic peak provides a measure of the width of the final state. Comparison with the $s+d$ LPDOS of Ga in Fig. 2 indicates that the sharp final state is probably associated with the prominent peak in the *s* density of states located at about 2.8 eV. This scattering process is illustrated in Fig. 9. Given this

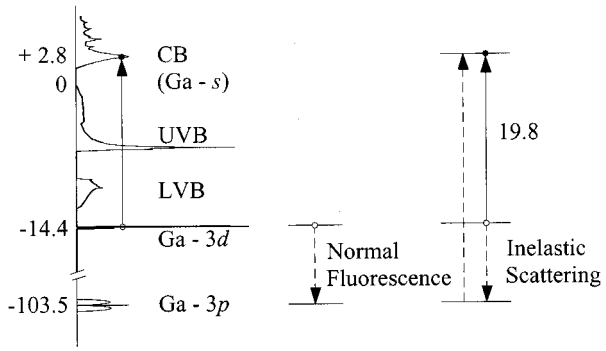

FIG. 9. Diagram of RIXS at Ga $M_{2,3}$ edge in GaP.

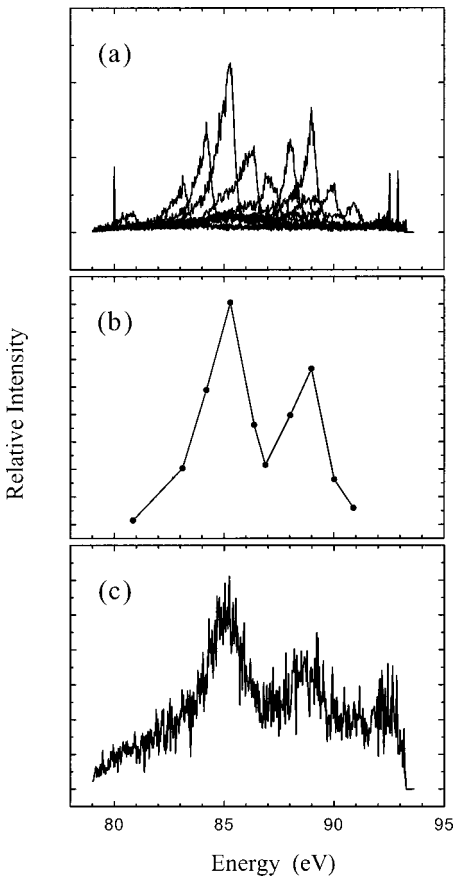

FIG. 10. Comparison of the intensities of RIXS peaks with normal fluorescent spectrum at the Ga $M_{2,3}$ edge in GaP. (a) An overlap of RIXS peaks at different exitation energies. (b) The dots represent different RIXS peaks in (a) and are connected together to compare with the normal fluorescent spectrum. (c) Normal fluorescent spectrum excited above the Ga $M_{2,3}$ edge.

interpretation, our experimental results indicate that the calculations underestimate the separation between Ga 3*d* bands and the conduction band by about 2.6 eV.

It is apparent from an overview of Fig. 8 that the RIXS spectrum is much narrower than the normal fluorescence spectrum at the Ga $M_{2,3}$ edge. This results from the RIXS feature in which the shape and energy position of the RIXS spectra are determined only by the distribution of the energy levels in the final state of the system. However, the characteristic features of RIXS spectra depend on materials. In many insulators, the excitation can occur between localized states associated with valence excitons or localized *d* and *f* states and yield effects similar to those observed here,[33,34] whereas in covalent solids such as crystalline silicon, diamond, and graphite, it is found that the crystal momentum is conserved in the scattering process.[35–38] We also note that the spectra have another interesting feature—the inelastic peak is prominent only within the range of the normal fluorescence spectrum and has an intensity that tracks the amplitude of the normal fluorescence spectrum. This characteristic is made clear in Fig. 10. This is another RIXS feature that is related to the lifetime broadening of the intermediate state of the scattering process. Thus, the different roles played by the intermediate and final states in the RIXS process are well represented in the Ga $M_{2,3}$ spectra of GaP.

ACKNOWLEDGMENTS

Experimental measurements were carried out at beamline 8.0 at the Advanced Light Source at Lawrence Berkeley National Laboratory. The research was supported by NSF Grant No. NSF-DMR-9801804 with the Univeristy of Tennessee. The ALS is supported by the Director, Office of Science, Office of Basic Energy Sciences, Materials Sciences Division, of the U.S. Department of Energy under Contract No. DE-AC03-76SF00098 at LBNL. The authors would like to thank the staff of the Joint Institute for Computational Science at the University of Tennessee for providing access to the IBM SP2 parallel supercomputer, and the valuable help of Dr. Melissa Grush and other collaborators on the soft x-ray fluorescent beamline 8.0 at the ALS.

[1] V.G. Aleshin and V.P. Smirnov, Fiz. Tverd. Tela (Leningrad) **11**, 1920 (1969) [Sov. Phys. Solid State **11**, 1546 (1970)].
[2] D.J. Stukel, Phys. Rev. B **1**, 4791 (1970).
[3] L.A. Hemstreet, Jr. and C.Y. Fong, Phys. Rev. B **6**, 1464 (1972).
[4] R.M. Wentzcovitch, K.J. Chang, and M.L. Cohen, Phys. Rev. B **34**, 1071 (1986).
[5] B.N. Onwuagba, Solid State Commun. **89**, 289 (1994).
[6] P. Rodríguez-Hernández, M. González-Diaz, and A. Muñoz, Phys. Rev. B **51**, 14 705 (1995).
[7] M.L. Cohen and T.K. Bergstresser, Phys. Rev. **141**, 789 (1966).
[8] M.L. Cohen and V. Heine, Solid State Phys. **24**, 37 (1970).
[9] J. Chelikowsky, D.J. Chadi, and M.L. Cohen, Phys. Rev. B **8**, 2786 (1973).
[10] J.R. Chelikowsky and M.L. Cohen, Phys. Rev. B **14**, 556 (1976).
[11] F. Bassani and M. Yoshimine, Phys. Rev. **130**, 20 (1963).
[12] A. Chen and A. Sher, Phys. Rev. B **22**, 3886 (1980).
[13] I. Singh and G.P. Srivastava, Phys. Status Solidi B **108**, 467 (1981).
[14] S.N. Sahu, J.T. Borenstein, V.A. Singh, and J.W. Corbett, Phys. Status Solidi B **122**, 661 (1984).
[15] J.P. Walter and M.L. Cohen, Phys. Rev. **183**, 763 (1969).
[16] C.S. Wang and B.M. Klein, Phys. Rev. B **24**, 3393 (1981).
[17] A.N. Gusatinskii *et al.*, Fiz. Tekh. Poluprovodn. **11**, 379 (1977) [Sov. Phys. Semicond. **11**, 218 (1977)].
[18] A.N. Gusatinskii *et al.*, Bull. Acad. Sci. USSR, Phys. Ser. **40**, 127 (1976).
[19] A.N. Gusatinskii and S.A. Nemnonov, Phys. Status Solidi **12**, 749 (1965).
[20] C. Sugiura, J. Phys. Soc. Jpn. **64**, 2510 (1995); **65**, 2170 (1996).
[21] P. Hohenberg and W. Kohn, Phys. Rev. **136**, B864 (1964).
[22] W. Kohn and L.J. Sham, Phys. Rev. A **140**, A1133 (1965).
[23] J.J. Jia *et al.*, Rev. Sci. Instrum. **66**, 1394 (1995).

[24] P. Blaha, K. Schwarz, and J. Luitz, *WIEN97, A Full Potential Linearized Augmented Plane Wave Package for Calculating Crystal Properties* (Karlheinz Schwarz, Techn. Universität Wien, Austria, 1999).
[25] J.P. Perdew, K. Burke, and M. Ernzerhof, Phys. Rev. Lett. **77**, 3865 (1996).
[26] P.E. Blöchl, O. Jepsen, and O.K. Anderson, Phys. Rev. B **49**, 16 223 (1994).
[27] L. Ley *et al.*, Phys. Rev. B **9**, 600 (1974).
[28] D.J. Chadi, M.L. Cohen, and W.D. Grobman, Phys. Rev. B **8**, 5587 (1973).
[29] L. Zhou *et al.*, Phys. Rev. B **55**, 5051 (1997).
[30] J. Tulkki and T. Åberg, J. Phys. B **15**, L435 (1982).
[31] J. Tulkki, Phys. Rev. A **27**, 3375 (1983).
[32] T. Åberg and B. Crasemann, in *Resonant Anomalous X-Ray Scattering: Theory and Applications*, edited by G. Materlik, C. J. Sparks, and K. Fischer (Elsevier/North-Holland, Amsterdam, 1994).
[33] W.L. O'Brien *et al.*, Phys. Rev. Lett. **70**, 238 (1993).
[34] J.J. Jia *et al.*, Phys. Rev. Lett. **76**, 4054 (1996).
[35] J-E. Rubensson *et al.*, Phys. Rev. Lett. **64**, 1047 (1990).
[36] K.E. Miyano *et al.*, Phys. Rev. B **48**, 1918 (1993).
[37] Y. Ma *et al.*, Phys. Rev. Lett. **69**, 2598 (1992).
[38] J.A. Carlisle *et al.*, Phys. Rev. Lett. **74**, 1234 (1995).